IOP Conference Series: Materials Science and Engineering

PAPER • **OPEN ACCESS**

Design, fabrication and test of high temperature superconducting magnet for heat flux and radio blackout mitigation experiments in plasma wind tunnels

To cite this article: S I Schlachter *et al* 2024 *IOP Conf. Ser.: Mater. Sci. Eng.* **1302** 012021

IOP Conf. Series: Materials Science and Engineering **1302** (2024) 012021 doi:10.1088/1757-899X/1302/1/012021

Design, fabrication and test of high temperature superconducting magnet for heat flux and radio blackout mitigation experiments in plasma wind tunnels

S I Schlachter[1], A Drechsler[1], R Gehring[1], M Eisele[1], F Gretschmann[1], F Hornung[1], S Westenfelder[1], J Willms[1], V Große[2], A Smara[2], M Dalban-Canassy[3], A Behnke[4], G Herdrich[4], J Oswald[4], A S. Pagan[4], B Helber[5], A Viladegut[5] and A Lani[6]

[1] Karlsruhe Institute of Technology, Institute for Technical Physics, 76344 Eggenstein-Leopoldshafen, Germany
[2] THEVA Dünnschichttechnik GmbH, 85737 Ismaning, Germany
[3] ABSOLUT SYSTEM SAS, 38170, France
[4] University of Stuttgart, Institute of Space Systems, Stuttgart, 70569, Germany
[5] von Karman Institute for Fluid Dynamics, Sint-Genesius-Rode, 1640, Belgium
[6] Katholieke Universiteit Leuven, Leuven, 3001, Belgium

Email: sonja.schlachter@kit.edu

Abstract. High heat flux and radio blackout are well-known challenges space vehicles have been facing during re-entry into a planet's atmosphere since the early days of space-flight. Thermal protection systems have been developed to protect spacecraft and astronauts, however, they are often heavy and some have to be replaced after each mission. High temperatures in the compressed gas in the shock wave lead to partial ionization. The dense plasma can cause radio blackout, i.e. attenuation or reflection of radio waves thus blocking data-telemetry and communication with ground stations or satellites. One approach to solve both problems is to influence the plasma with magnetohydrodynamic effects using a strong magnet. In the framework of the European project MEESST (Magnetohydrodynamic Enhanced Entry System for Space Transportation) heat flux mitigation and radio blackout mitigation is investigated by means of modelling and ground experiments in plasma wind tunnels at the Institute of Space Systems (Stuttgart, Germany) and at the Von Karman Institute for Fluid Dynamics (Brussels, Belgium) using an HTS magnet. After a short introduction to the scientific background of the MEESST project, the boundary conditions for the design of the magnet and calculations of field distributions are presented. The pancake coils of the magnet were wound with a robotic winding system. Results from a preliminary test of the conduction-cooled magnet are presented.

1. Introduction

Entering the atmosphere of a planet at high velocity poses major challenges for spacecraft. High heat fluxes caused by the compressed and partially ionized gas at the leading edge of the spacecraft can heat the surface to temperatures, which can significantly exceed the operational temperatures of the structure materials. A thermal protection system (TPS), e.g. with ablative heat shields as in the Mercury, Apollo and Gemini missions or with radiatively-cooled heat shields as used on the Space Shuttle, is necessary

to protect the spacecraft from the high heat fluxes. However, these systems are often heavy and fragile. In 2003 a failure of the TPS of the Space Shuttle Columbia ended in the death of the seven astronauts. Pieces of insulating foam broke from the external fuel tank during launch and damaged the TPS at the left wing [1].

Another problem that is well known since the early days of space exploration is the radio-blackout phenomenon. The partially ionized gas in the plasma can block radio waves and lead to a loss of GPS data telemetry or communication with ground stations. Blackout occurs when the radio waves used for communication between ground stations and satellites are attenuated and/or reflected by the plasma layer that is created during hypersonic or re-entry flight. Some space capsules, e.g. Gemini, Mercury or Apollo missions, experienced radio blackout phases lasting up to several minutes during re-entry or hypersonic flight [2]. More than half a century later, this problem still exists for many missions and even though there are some ideas how the radio blackout can be mitigated by passive or active methods [3], effectively working solutions are still needed.

Radio wave transmission is possible at radio wave frequencies greater than the plasma frequency, which is related to the plasma number density [4]. One approach to solve the radio blackout problem is reduction of the density of the plasma layer in the vicinity of senders or antennas by magneto-hydrodynamic (MHD) effects.

In the framework of the European project MEESST (Magnetohydrodynamic Enhanced Entry System for Space Transportation) we have developed a high temperature superconducting (HTS) magnet for ground experiments in plasma wind tunnels to demonstrate that both, heat flux mitigation and radio blackout mitigation can be achieved by magnetohydrodynamic (MHD) effects. The magnet and its cryogenic system have been designed to fit in a probe that will be installed in plasma wind tunnels at the Institute of Space Systems (IRS) of the University of Stuttgart, Germany, for heat flux mitigation experiments, and at the von Karman Institute (VKI) for Fluid Dynamics in Brussels, Belgium, for radio blackout mitigation experiments. The Scientific goals of the MEESST project, the consortium and the roles of the partners within the MEESST project are described in more detail in Ref. [5].

In this paper we briefly review the design of the magnet and the cryogenic system (section 2) and describe how the magnet was manufactured with help of a robotic winding facility at KIT, the Karlsruhe Institute of Technology (section 3). In section 4 the results of the magnet test will be presented and discussed.

2. Magnet and cryogenic system design

Heat flux mitigation and radio blackout mitigation experiments will be performed in two different plasma facilities at IRS and VKI, respectively. The cryostat with the magnet is currently being installed in a probe that will be placed in the plasma beams during experiments. The probe has a warm bore located in the central axis of the magnet, which will host analytical devices to control the plasma parameters during the experiments. The front of the probe is water cooled to reduce the temperatures during plasma experiments, especially when magnetic fields are low.

2.1. Cryogenic system

The cryogenic system design and assembly has been performed by Absolut Systems (AS) in close cooperation with the project partners. The HTS magnet will be conduction cooled by connecting it to a cooling plate that is cooled with helium gas flowing through a spiral heat exchanger. A coldbox with a Cryomech AL325 coldhead, the compressor, vacuum pumps, the magnet power supply and the data acquisition and control unit will be placed in ambient conditions outside the plasma chamber. The cold helium gas is transferred via cryogenic lines from the cold box to the spiral cooling plate heat exchanger and back. Details of the experimental setup, especially for the heat flux mitigation experiments at IRS can be found in [6]. The cooling system has been designed to cool the HTS magnet to temperatures around 30 K. First tests of the cryogenic system indicated that the minimum achievable temperatures are even lower, allowing a higher safety margin for the operation of the superconducting magnet.

2.2. Magnet

The HTS magnet was designed to produce a magnetic field in the range of 1-2 Tesla at the front surface of the probe, which has a warm bore to accommodate measurement equipment. The following technical and economical boundary conditions had to be taken into account during the design process:

- the geometric design of the probe, including a curved front surface of the probe, a warm bore with a diameter of 30 mm, and a limited outer diameter, in order to be compliant with the requirements of the plasma experiments.
- limited cooling power, especially regarding current lead losses.
- limited budget for superconducting REBCO material, allowing a design with either 300 m of 12 mm wide or 900 m of 4 mm wide REBCO tape.

In order to ensure a high winding density and a safe operation of the conduction cooled magnet, it was decided to use a no-insulation (NI) magnet design. The NI magnet design allows current and heat transfer not only along the superconducting tape, but also perpendicular to the tape surface. For fast ramped or ac magnets the NI design is not beneficial, because high *L/R* ratios (*L*: conductance, *R*: turn-to-turn resistance) cause part of the current to flow through the normal conducting components of the HTS tape perpendicular to the winding rather than staying in the superconducting layer during ramping. Time constants for reaching a stable field value, which corresponds to the state in which the current flows in the superconducting layer along all windings, can easily be in the range of several seconds to minutes, depending on the inductance and the inter-winding resistance [8]. As fast ramping or ac operation is not required during the plasma experiments with the MEESST magnet, the NI magnet approach is advantageous compared to a design with insulation between the superconducting tapes.In contrast to many other superconducting magnet, not the central magnetic field in the bore of the magnet, but the field inside the plasma in front of the probe is of interest for the plasma experiments in the MEESST project. Therefore, it was important to bring the magnet windings as close as possible to the curved front of the probe head. A magnet design with several pancake coils (PCs) was chosen due to the required magnet geometry with a short magnet length to bring the windings close to the plasma and the rather high winding thickness to make use of the available conductor length. Layer winding was not anticipated due to the high number of necessary edge transitions. During the design phase, several designs with either 12 mm or 4 mm wide tape, varying pancake number and even with varying outer diameter of the pancake coils within the magnet were analysed to account for the curved probe front surface. Magnetic field calculations were performed with COMSOL® and Matlab® using angle, temperature and field dependent critical current data for THEVA (Ismaning, Germany) tapes from Ref. [8]. Screening currents have not been taken into account, i.e. a uniform current distribution was assumed. Figure 1 shows the radial magnetic field distribution $|\boldsymbol{B}|(x, d)$ in distances of d = 10 mm (black), 20 mm (red), 30 mm (green) and 40 mm (blue) away from the winding end of the pancake closest to the plasma for design currents of 70% of $I_c(T = 30\ \mathrm{K})$ as listed in table 1. All magnet configurations have been calculated for a total conductor length of 900 m and a conductor width and thickness of 4 mm and 75 µm, respectively. In each case the inner winding radius has been set to R_i=33 mm, to account for the space needed for the warm bore, cryostat and magnet core. The distance between single pancakes is 0.6 mm, accounting for electrically insulating spacers. Calculations have been performed for different coil designs with either 5 pancake coils with equal inner and outer diameter (design A, filled symbols), five PCs with same inner, but different outer diameter (design B, open symbols) and 4 PCs with different inner and outer diameter (design C, lines). It turned out that the magnetic fields that are achievable outside the windings are not much different for the different geometries. The lowest fields were obtained for the design with 5 PCs with different outer diameters. Especially at larger radial distances from the central axis, the magnetic fields for the design with 5 equal PCs showed the highest magnetic field values. The magnets with smaller outer winding diameter could be brought a bit closer to the plasma due to the curved nature of the plasma probe and the cryostat. However, the field enhancement would not be very large, and stabilizing the windings against Lorentz forces during operation would be more challenging than for a magnet with equally sized PCs.

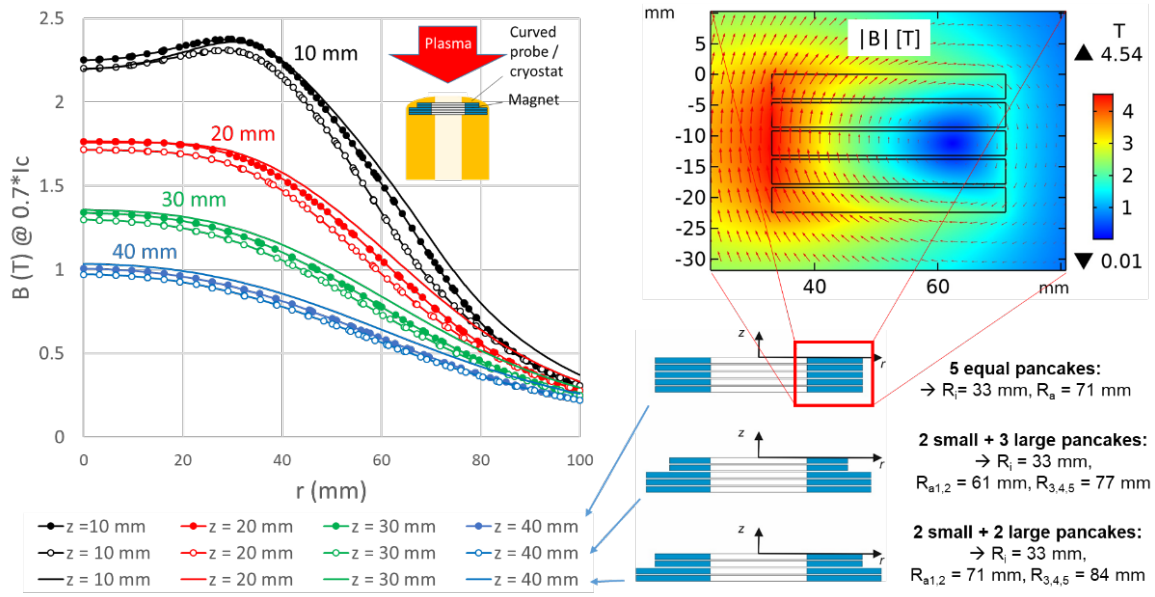

Figure 1. Radial magnetic field distribution $|\boldsymbol{B}|(r, d)$ in distances of $d = 10$ mm, 20 mm, 30 mm and 40 mm away from the winding end of the pancake closest to the plasma for design currents of $I = 0.7 \cdot I_c(T = 30\ \text{K})$ with $I_c(T = 30\ \text{K})$ as shown in table 1. Calculations have been performed for different coil designs with either 5 pancake coils with equal inner and outer diameter (design A, filled symbols), five PCs with same inner, but different outer diameter (design B, open symbols), and 4 PCs with different inner and outer diameter (design C, lines). The field distribution and direction in the winding-pack cross section of design A for $I = 0.7 \cdot I_c(T = 30\ \text{K})$ is shown in the upper right graph. All magnet configurations have been calculated for a total conductor length of 900 m and a conductor width and thickness of 4 mm and 75 µm, respectively. The distance between single pancakes is 0.6 mm, accounting for electrically insulating spacers.

In table 1 we have listed inner and outer radii ($R_{i,n}$ and $R_{a,n}$) of pancakes PCn, (n = 1-5), calculated critical currents I_c, and the maximum magnetic fields at the conductor B_{max} for the three different coil designs which were presented in figure 1. The critical currents for designs A, B and C at $T = 30$ K are $I_{c,A} = 125.9$ A, $I_{c,B} = 126.6$ A and $I_{c,C} = 129.7$ A, respectively. The reason for the different I_c values of the different magnets, are the maximum magnetic fields that are achieved at the conductor.

Table 1. Inner and outer radii of PCs for different magnet designs as presented in figure 1, critical currents at design temperature of 30 K and maximum magnetic field at the conductor.

# of PCs	R_i (mm)	$R_{a1,2}$ (mm)	$R_{a3,4,(5)}$ (mm)	$I_c(T$=30 K) (A)	$B_{max,\ Conductor}$ (T)
5	33	71	71	125.9	6.32
5	33	61	77	126.6	6.27
4	33	71	84	129.7	6.04

Figure 2 shows a cross section of the magnet installed in the cryostat. The cryostat is installed in the probe and has also a curved front shape. The maximum distance between the winding end and the outer surface of the probe is approximately 25 mm. During plasma experiments the magnet will only be driven with maximum currents of approximately 70% of the critical current in order to prevent it from quenching, so according to the magnet design a maximum field of the order of 1.5 T can be achieved at the design temperature of 30 K.

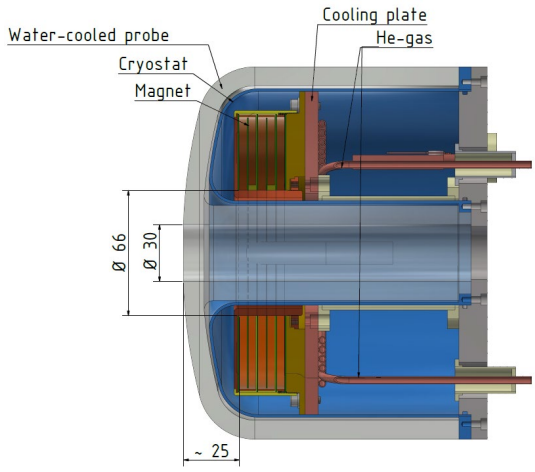

Figure 2. CAD design of MEESST magnet mounted in cryostat and plasma probe. All dimensions are in mm.

2.3. HTS tapes for magnet winding and joints

The above-mentioned magnetic field calculations were made with angular dependent $I_c(B,T)$ data for a THEVA ProLine tape with a self-field (s.f.) critical current of I_c(77K, s.f.) = 168.6 A. The tapes for the MEESST magnet produced by THEVA have a minimum critical current of $I_{c,min}$(77K, s.f.) = 146.6 A, which is 13% lower than that used for the field calculations. It is thus assumed in a first approximation that the 3 different designs of the MEESST magnet will only achieve 87% of the magnetic field values shown above. However, the THEVA tapes are rather inhomogeneous with a maximum critical current of $I_{c,max}$(77K) = 314.7 A and an average critical current of $I_{c,avg}$(77K) = 236.1 A. As all tapes are connected in series, the minimum critical current in the conductor determines the maximum field that can be achieved. However, as the critical currents in the magnet are field dependent, the section with the lowest critical current in self-field is not necessarily the section with the lowest critical current in the magnet due to the inhomogeneous field distribution. Therefore, the worst tapes were placed in a low-field section of the magnet, i.e. in the outer part of the the pancakes P2- P4. An overview of the 4 mm wide REBCO tapes that were available for winding the MEESST magnet is given in table 2.

According to the magnet design, a total tape length of 180 m would have been required for each pancake. However, only one of the delivered tapes had a length of 180 m. This tape was used to wind

Table 2. Overview of length, minimum, maximum and average critical current of the 4 mm wide REBCO tapes available for winding the different PCs in the magnet. The tapes have a nominal thickness of ~75 µm (substrate: 50 µm; Cu surround: 10 µm; total thickness of buffer, REBCO and Ag layer ~ 5 µm).

		Pancake 1	Pancake 2	Pancake 3	Pancake 4	Pancake 5
Outer part of PC	ID		ID22006-1	ID22010	ID22006-2	ID22011
	Length		60 m	60 m	60 m	60 m
	$I_{c,min}$		152.8 A	146.6 A	152.8 A	161.6 A
	$I_{c,max}$		262.1 A	249.2 A	262.1 A	245.6 A
	$I_{c,avg}$		225.4 A	218.7 A	225.4 A	211.3 A
Inner part of PC	ID	ID22004	ID22005	ID22008	ID22009	ID22007
	Length	180 m	120 m	120 m	120 m	120 m
	$I_{c,min}$	158.4 A	155.9 A	188.5 A	174.7 A	154.9 A
	$I_{c,max}$	258.3 A	265.7 A	309.1 A	314.7 A	252.9 A
	$I_{c,avg}$	224.1 A	234.2 A	269.3 A	284.3 A	221.4 A

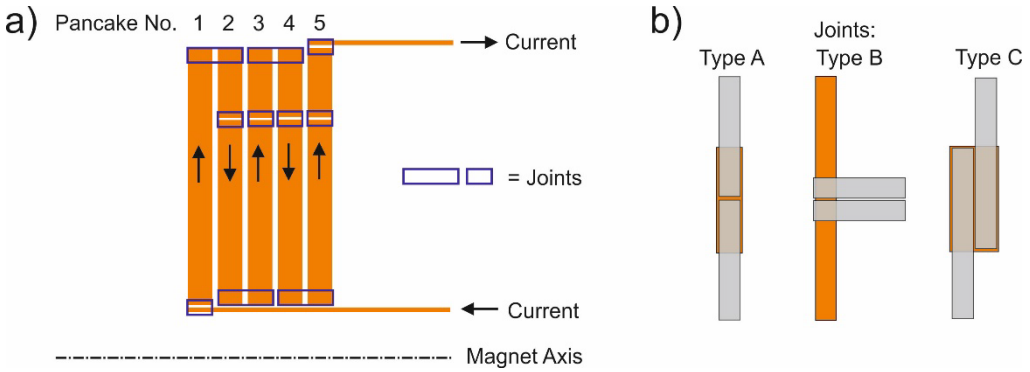

Figure 3. a) Position of joints to connect tapes in MEESST magnet and current flow. Only the upper half of the winding pack is shown, the magnet central axis is indicated at the bottom of the figure. b) Sketch of three different joint types as described in the text.

PC 1 which is the PC closest to the plasma and therefore farthest away from the cooling plate. In addition to the 180 m long tape, five 120 m long tapes and three 60 m long tapes were delivered. One of the 120 m long tapes was cut in two halves so that for each of the PCs 2-5 a 120 m and a 60 m long tape could be used. Due to the limited length of the available tapes a total number of 10 joints was necessary to connect all tapes in series and to connect PC1 and PC5 to the current leads. A schematic representation of the tape and joint arrangement and the current path is given in figure 3.

Three different types of joints were used for the MEESST magnet. All joints were soldered with In97Ag3 solder and a soldering device in which the tapes were pre shaped with a radius, so that they did not have to be bent too much during the winding process:

- type A: bridge type joints to connect the inner and outer tape within one pancake, keeping the orientation of the REBCO layer constant so that all PCs could be wound in compressive mode,
- type B: 90° face-to-face type joints to connect two 4 mm wide current-lead tapes to PC 1 and two 4 mm wide current lead tapes to PC 5,
- type C: bridgetype joints with 8 mm wide bridge tapes to connect the tapes of neighbouring PCs side by side at the inner or outer radius of the coil. The bridge tapes were cut with a pico-second laser out of a 12 mm wide tape. After laser cutting, the 12 mm wide bridge tape was electroplated with a thin Cu layer to close the open sides of the tape after laser cutting.

3. Magnet manufacturing

Coil winding was performed at KIT with a robotic winding facility (figure 4). Before starting the winding process, the 120 m and 60 m long tapes for PCs 2-5 were joined, so that a total tape length of 180 m was available for each pancake. The full 180 m length of tape required for each of the five PCs was wound on a separate spool. In a next step the two current lead tapes for PC1 were soldered face-to-face to the PC1 tape. A special holder for the magnet former was manufactured and held by robot #1. Two other robots were available to hold the two supply spools necessary for winding a double pancake (two pancakes with joint at the inner radius). The robots were programmed to allow a high flexibility in adjusting movements and tape positions. Winding numbers were counted automatically. The winding tension could be changed by adjusting the current of a torque motor.

After winding PC1 an insulating G10 plate was placed on the pancake side towards PC2. Then the tapes for PC2 and PC3 were joined side-by-side with a bridge-type joint. PC2 was wound while the supply spool with the tape for PC3 was kept in a fixed position relative to the magnet. After winding PC2 a Cu-ring with slits to lead the winding ends out was placed over PC1 and PC2. The Cu ring helps to avoid radial movement of the winding in case of hoop stress. Furthermore it is used as a parallel shunt for the outer joint connecting PC1 and PC2. The outer joints were soldered after completing the winding process. In a next step a further G10 plate was placed on the side of PC2 facing PC3 and then PC3 was

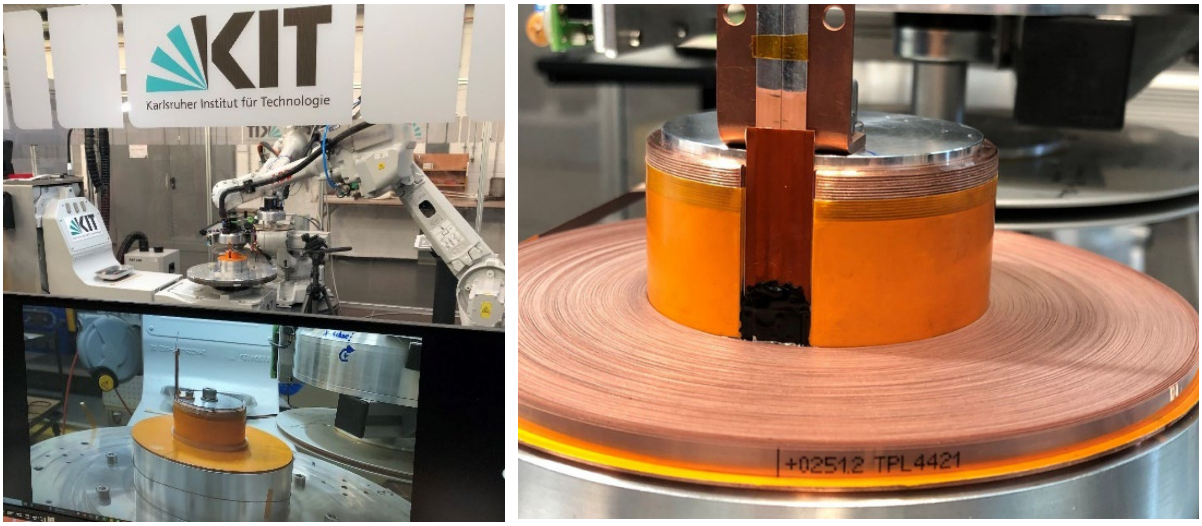

Figure 4. Winding of PC1 at KIT's robotic winding facility (left) and PC1 after winding (right).

wound. Winding of PC4 and PC5 was performed in a similar way with insulating G10 plates between the pancakes and Cu rings connecting PC3 and PC4 at the outer radius of the magnet. After winding PC 5, two current lead tapes were soldered in a 90° angle face-to-face to PC5. In final steps the outer joints connecting PC1 to PC2 and PC3 to PC4 were soldered and voltage taps were soldered to the outer surface of the pancakes and current leads (figure 5).

While the winding process with the robots is very convenient and coil and supply spool positions can precisely be controlled, it turned out that the winding numbers were far below the theoretical value of 511 turns expected from the geometric data. In an initial winding process for PC1 only 389 windings could be placed on the former. As winding had been performed with a very low winding tension of about 3 MPa, PC1 was unwound and then rewound with an approximately 5 times higher tension. However, also with much higher winding tension only 391 windings could be achieved. Exactly the same winding number was achieved for PC2, while for PC3, PC4 and PC5 winding numbers of 457, 459 and 423, respectively, could be achieved. The reason for the strongly differing winding numbers is a difference in the conductor quality. Some of the tapes were from earlier batches for which the laser cutting process to cut 4 mm wide tapes out of 12 mm wide tapes had not been optimized at the time of tape fabrication. They showed thick precipitates on one edge of the conductor that increased the thickness at this edge to

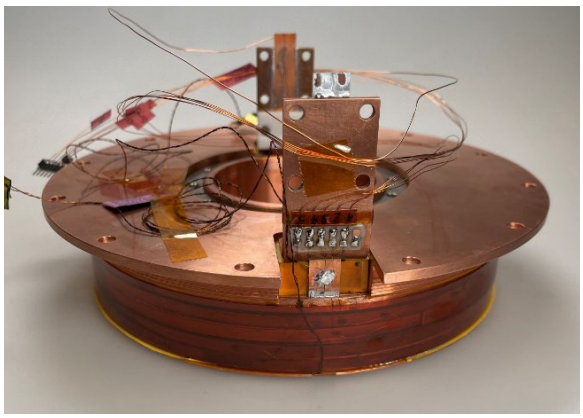

Figure 5. MEESST magnet after winding and attaching voltage taps. Two Cernox sensors are placed close to PC1 winding (plasma side) and close two PC5 winding (cooler side). The magnet is ready for test.

Figure 6. Optical image with a view on the side of the tape used for winding PC1. Large precipitates can be seen on the tape surface, leading to a strong increase of the effective conductor thickness in the winding.

values in the range of 90-100 µm (figure 6). Stacking of these faults led to the low winding number and consequently to voids in the remaining sections between adjacent windings. It was clear that the voids might lead to problems, because of poor and unpredictable thermal and electrical contact. Hoop stress could lead to radial conductor movement and tensile stress on conductors and joints. Unfortunately, due to the tight schedule and the limited budget the MEESST project did not allow to rewind the magnet with improved conductors.

4. Magnet test results

Before delivery of the magnet to AS and installation in the MEESST cryostat, a magnet test was performed at KIT. For this test, the MEESST magnet was mounted to a cryo-cooled insert of a large cryostat with an outer diameter of 80 cm.

After cooling the magnet to temperatures below 30 K, first tests with ramps to low currents and back to zero were performed. Figure 7 shows current and the measured voltages for different sections of the magnet. Voltage taps have been soldered to current leads and PCs at positions as indicated schematically in figure 8. The voltage $U_{\mathrm{CL\text{-}PC1}}$ consists of an inductive contribution from PC1, visible during ramping, and a resistive contribution from the joint connecting current leads and PC1. The voltages $U_{\mathrm{PC1\text{-}PC2}}$ and $U_{\mathrm{PC3\text{-}PC4}}$ are mainly due to the resistive contributions due to the joints connecting the pancakes at the outer circumference of the magnet. During ramping the voltages $U_{\mathrm{PC2\text{-}PC3}}$ and $U_{\mathrm{PC4\text{-}PC5}}$ show inductive contributions from two pancakes and resistive contributions from joints inside the PCs and connecting the PCs. Furthermore, the resistive contribution to $U_{\mathrm{PC4\text{-}PC5}}$ includes a contribution from the joint between PC5 and the current lead that is soldered to it. As expected, the inductive contribution of PC1 is only about half the value as for the voltages $U_{\mathrm{PC2\text{-}PC3}}$ and $U_{\mathrm{PC4\text{-}PC5}}$ which contain two pancakes. Similar measurements have been performed with ramps to higher currents. The inductance of the magnet was estimated from the measurements with current ramp $\mathrm{d}I/\mathrm{d}t = 0.02$ A/s to 5 A, giving a value of 367 mH.

Measurements of the magnetic field were performed with hall probes mounted in the center of the magnet and in a distance of 20 mm from the winding end on the magnet axis and were then compared to values obtained from simulation. Figure 9 shows a very good agreement between measured and calculated data for currents of 5 A, 20 A and 50 A.

When we tried to increase the current to 70 A, a quench occurred slightly above 62 A (figures 10 and 11). An increase of $U_{\mathrm{PC2\text{-}PC3}}$ during the ramp to 50 A was already observed before the quench, indicating a large resistive contribution. At constant current $I = 50$ A, the voltage $U_{\mathrm{PC2\text{-}PC3}}$ was ~ 0.96 mV, corresponding to a resistance of $R = 19$ µΩ in the magnet section of PC2 and PC3 which includes 3 joints. The resistive contributions determined from $U_{\mathrm{CL\text{-}PC1}}$, $U_{\mathrm{PC1\text{-}PC2}}$, $U_{\mathrm{PC3\text{-}PC4}}$ and $U_{\mathrm{PC4\text{-}PC5}}$ were 174 nΩ

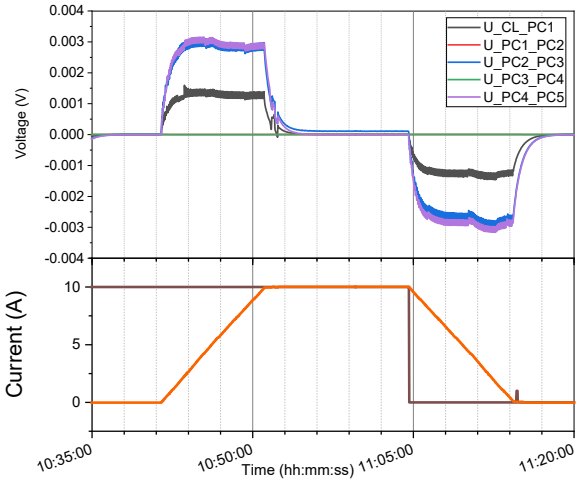

Figure 7. a) MEESST magnet voltages and b) current during a ramp to 10 A.

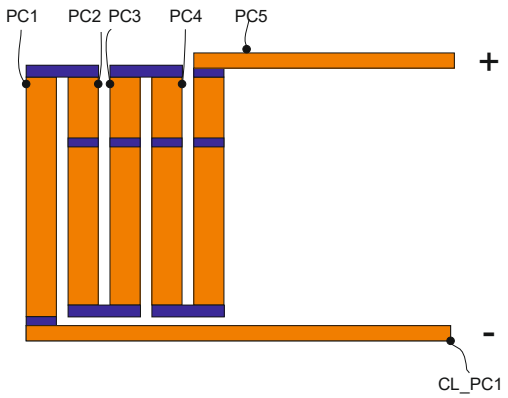

Figure 8. Schematic illustration of voltage tap positions at PCs and current leads.

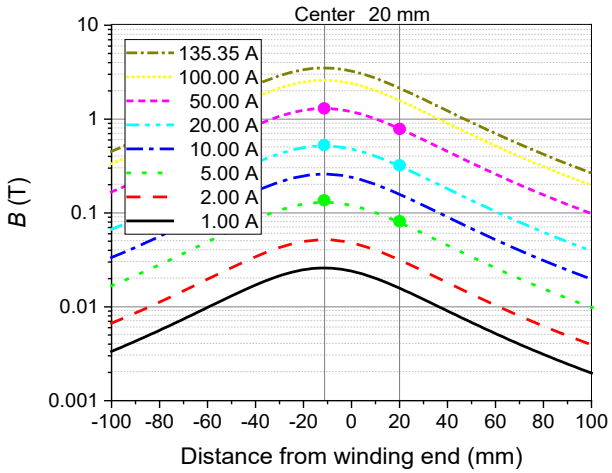

Figure 9. Calculated magnetic field strength B along the central axis of the MEESST magnet for different currents (lines) and measured values in the center of the magnet and 20 mm away from the winding end.

(including 1 PC and 1 joint), 33.4 nΩ (including 1 joint), 34 nΩ (including 1 joint), and 280 nΩ (including 2 pancakes and 4 joints), respectively. The temperatures measured at the cooler side of the magnet, close to the winding of PC5 and the current lead temperatures did not increase much before the quench, whereas a strong increase from 20.3 K to 22.7 K directly before the quench was observed at the plasma side of the magnet, close to the winding of PC1.

It is not clear which of the 3 joints in the magnet section PC2-PC3 led to the quench of the magnet, or if even a defect in the winding caused the problem. During handling of the tapes we had observed that they tend to delaminate very easily, so applying tensile force to joints, for example, might have caused delamination and therefore high joint resistance. The high void fraction in the PCs with low winding number might have led to outward movement of the tape with applied current. This can also lead to tensile stress and delamination, especially in the joint sections.

As the magnet is necessary to achieve the objectives of the MEESST project in plasma experiments, we tried to see if it can still be used - maybe with lower current as originally anticipated. Therefore, we increased the temperatures of the magnet to approximately 30 K, the design temperature of the cryogenic system, and applied a current of 50 A with slow current ramps and hold times of a few minutes at 20, 25, 30, 35, 40, and 45 A. We held the magnet at I = 50 A for 45 minutes and then decreased the

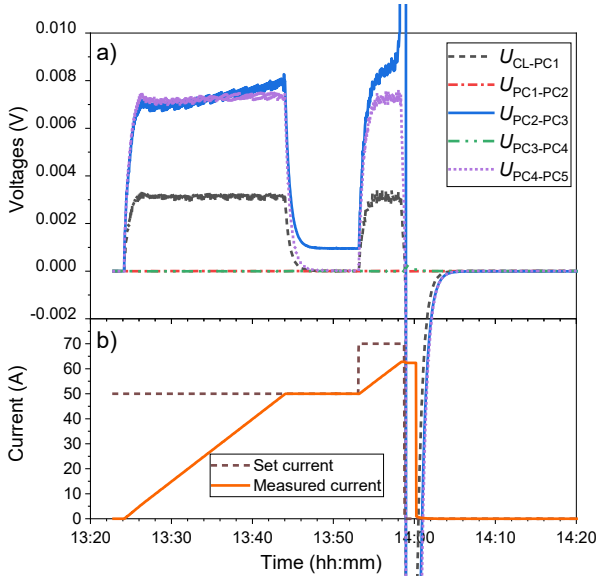

Figure 10. a) MEESST magnet voltages and b) current during a ramp to 50 A and then to 70 A. Before reaching 70 A, a quench occurred.

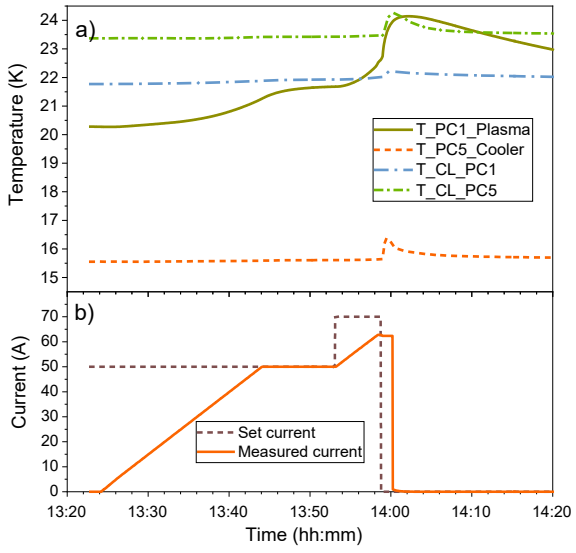

Figure 11 a) MEESST magnet temperatures and b) current during same measurement as in figure 10.

temperature of the magnet until all sensors were below 25 K. We kept it at 50 A for about 1 hour after we started to decrease the temperature and then decreased it slowly to zero. It seems that the magnet can be operated at this reduced current so that magnetic fields of approximately 0.7 T can be achieved in the plasma.

5. Conclusions and outlook

An HTS magnet has been designed and built for plasma experiments in the framework of the European MEESST project. It consists of five PCs that were wound in KIT's robotic winding facility. Due to the limited length of REBCO tapes and to connect the current leads, a high number of solder joints was necessary to connect the tapes in series. The achieved winding number was much lower than expected from geometry, mainly due to inhomogeneous thickness of the tapes.

During the test of the conduction-cooled magnet, a quench occurred at $I \sim 62$ A – much below the estimated critical current of the magnet. A high resistance was observed in magnet section PC2-PC3 which includes 2 pancakes and 3 soldered joints. There could be either a defect in one of the joints, e.g. caused by delamination during winding or due to Lorentz forces or even a defect in the winding.

Nevertheless it could be shown that the magnet can be operated at 30 K with a current of 50 A. With this current, it is possible to achieve a magnetic field of approximately 0.7 T outside the cryostat and probe in the plasma during heat flux mitigation and radio blackout mitigation experiments that will be conducted in 11/2023 and 01/2024 at VKI and IRS, respectively.

Meanwhile Theva was able to improve their tape quality so that a magnet in a possible follow-up project could be improved.

6. References

[1] McDanels S J, Mayeaux B M, Collins T E, Jerman G A, Piascik R S, Russell R W, and Shah S R 2006 An overview of the space shuttle Columbia accident from recovery through reconstruction; Journal of Failure Analysis and Prevention 6 pp 82-91

[2] Rogers L 2008 *It's only rocket science: an introduction in plain English.* Astronomers' universe: Springer eBooks collection. Springer. pp. 159–162. ISBN 978-0-387-75378-2

[3] Hartunian R A, Stewart G E, Curtiss T J, Fergason S D, Seibold R W and Shome P 2007 Implications and Mitigation of Radio Frequency Blackout During Reentry of Reusable Launch Vehicles, AIAA Atmospheric Flight Mechanics Conference and Exhibit 20 - 23 August 2007, Hilton Head, South Carolina, DOI: 10.2514/6.2007-6633

[4] Rybak J P and Churchill R J 1971 Progress in re-entry communications *IEEE Trans. on Aerospace and Electronic* aes-7 879–894

[5] Lani A *et al. 2023* A Magnetohydrodynamic enhanced entry system for space transportation: MEESST *Journal of Space Safety Engineering* 10 pp. 27-34

[6] Oswald J W, Mall V, Behnke A, Pagan A S, Dalban-Canassy M, Schlachter S, Gehring R, Sharma V, Lani A, and Herdrich G. 2023 MHD Flow Manipulation Experiments in High Enthalpy Air Plasma; submitted to proceedings of 34th International Symposium on Space technology and Science (ISTS), June 3-9, 2023, Kurume City, Japan

[7] Xudong Wang, Seungyong Hahn, Youngjae Kim, Juan Bascuñán, John Voccio, Haigun Lee, Yukikazu Iwasa 2013 Turn-to-turn contact characteristics for an equivalent circuit model of no-insulation ReBCO pancake coil *Supercond. Sci. Technol*. 26, 035012

[8] Wimbush S C and Strickland M N 2017 IEEE Trans. Appl. Supercond. 27 8000105
Wimbush S and Strickland N 2016 A high-temperature superconducting (HTS) wire critical current database. figshare. Collection. https://doi.org/10.6084/m9.figshare.c.2861821.v12

Acknowledgment

The MEESST project has received funding from the European Union's Horizon 2020 research and innovation program under grant agreement No.899298.